RSC Advances

PAPER

View Article Online
View Journal | View Issue

Cite this: *RSC Adv.*, 2024, **14**, 75

Understanding the role of solvents in bottom-up synthesis of multi-element hydroxides†

Fei Li, *[a] Kanako Yoshida,[a] Nguyen Van Chuc, [b] Minoru Osada[c] and Hiroya Abe*[a]

Received 28th October 2023
Accepted 11th December 2023

DOI: 10.1039/d3ra07344k

rsc.li/rsc-advances

Here we report a comparative study on the bottom-up synthesis of multi-element hydroxides composed of Mg, Al, Fe and Zn cations to understand the role of solvents. Two common solvents, water and ethylene glycol, a typical polyol, are used. The polyol-derived MgAlFeZn–OH are nanosheets with homogeneous elemental distribution, while the hydrothermal-derived MgAlFeZn–OH are mixtures of plate-like hydroxide layers and rod-like spinel oxides. The coordinating properties and the high viscosity of the ethylene glycol provide the possibility to mediate the hydrolysis rates and to control the particle growth. The high specific surface area of the polyol-derived multi-element hydroxide nanosheets (352.4 $m^2\ g^{-1}$) guarantees them as excellent adsorbents for adsorbing anionic dyes in aqueous solution.

1. Introduction

Layered double hydroxides (LDHs) are a class of synthetic clays that have the brucite $Mg(OH)_2$-like structure, where the divalent metal cations are partially substituted by high-valence (typically trivalent) metal cations.[1–3] LDHs have the general formula $[M^{2+}_{1-x}M^{3+}_{x}(OH)_2]^{x+}[A^{n-}]_{x/n}\cdot yH_2O$, where M^{2+} is the divalent metal cation, M^{3+} is the doping trivalent cation, A^{n-} is the counter anion that keeps charge balance, and x is the mole fraction of the trivalent cation.[1,2] The divalent metal cations can be Mg^{2+}, Fe^{2+}, Co^{2+}, Ni^{2+}, Cu^{2+} or Zn^{2+}, while the trivalent metal cations can be Al^{3+}, V^{3+}, Cr^{3+}, Mn^{3+} or Fe^{3+}.[1] The unique positively charged layered structures of LDHs and their good compositional flexibility find themselves wide applications in broad areas, such as catalysts for water splitting and adsorbents for dye removal.[3,4] Besides using binary metal cations, researchers have introduced the third and even the fourth trivalent metal cations in low proportions into the LDH matrix materials to form ternary LDHs and quaternary LDHs, respectively, in order to improve their performance.[5,6] However, it has been widely accepted that the solubility limit of $x = M^{3+}/(M^{2+} + M^{3+})$ is around 0.33 in LDHs.[1,2]

The high-entropy design concept, *i.e.*, creating materials by increasing configurational entropy as a driving force, has been introduced to the two-dimensional hydroxides in 2020–2022.[7–18] In high-entropy materials, four or more metal species in equimolar or near equimolar ratios are mixed together to form a single-phase crystal structure. The high-entropy concept extends the solubility limit in LDHs.[19–23] In the high-entropy hydroxides, there are no dominating cation species, and each metal cation species can be considered as the host cations. First-row transition metal elements such as Cr, Mn, Co and Ni are commonly chosen to obtain high-entropy hydroxides with improved performance.[20,21,24,25] When the transition metal cations were homogeneously mixed at nanoscale, the difference in electronegativity among these transition metal elements resulted in the charge transfer to regulate their electronic structures.[25,26] The corresponding electron-rich or electron-deficient cation sites would be the active sites for many potential applications.[25,26] However, these transition metal elements are toxic, even though they are earth-abundant.[27–33] Very few works focus on the synthesis and applications of the high-entropy hydroxides containing only non-toxic metal cations.[34]

Several bottom-up methods such as hydrothermal, solvothermal and electrochemical processes have been reported to synthesize high-entropy hydroxides.[20,22,35–38] Solubility product constant (K_{sp}) is one of the key factors when synthesizing materials from reactions in solutions.[39] The homogeneous precipitation of the targeted elements is a sufficient condition for the formation of high-entropy materials.[8,9,40] How to obtain uniform precipitates with multiple metal species differing greatly in K_{sp} is an important technical issue in synthesizing high-entropy hydroxides. Solvents are supposed to play vital roles in synthesizing high-entropy hydroxides *via* solution-based bottom-up processing. In this work, we report the comparative study on the synthesis of multi-element hydroxides composed of Mg, Al, Fe and Zn cations to understand the role of solvents. MgAl LDHs are benchmark compositions in conventional LDHs.[1] Fe and Zn cations are less toxic compared to the other transition metal cations. These four metal cations have

[a]*Joining and Welding Research Institute, Osaka University, Osaka 5670047, Japan. E-mail: feili@jwri.osaka-u.ac.jp; h-abe@jwri.osaka-u.ac.jp*

[b]*Institute of Materials Science, Vietnam Academy of Science and Technology, Hanoi, Vietnam*

[c]*Institute of Materials and Systems for Sustainability, Nagoya University, Nagoya 4648603, Japan*

† Electronic supplementary information (ESI) available. See DOI: https://doi.org/10.1039/d3ra07344k

largely different K_{sp} values in aqueous solutions.[41] The polyol process with ethylene glycol as solvent and hydrothermal process with water as solvent are applied. The phase, microstructure and elemental homogeneity of the multi-element hydroxides MgAlFeZn–OH are investigated. The polyol-derived MgAlFeZn–OH are nanosheets with homogeneous elemental distribution, while the hydrothermal-derived MgAlFeZn–OH are mixtures of plate-like hydroxide layers and spinel oxides. As one of the potential applications, these multi-element hydroxides can be used as the adsorbents for anionic dyes such as Congo red removal from the wastewater.

2. Experimental

Magnesium nitrate hexahydrate ($Mg(NO_3)_2 \cdot 6H_2O$), aluminum chloride hexahydrate ($AlCl_3 \cdot 6H_2O$), zinc nitrate hexahydrate ($Zn(NO_3)_2 \cdot 6H_2O$), potassium carbonate (K_2CO_3, anhydrous), Congo red (CR, $C_{32}H_{22}N_6Na_2O_6S_2$), and ultrapure water for LC/MS were purchased from FUJIFILM Wako Pure Chemical Corporation, Osaka, Japan. Iron(III) nitrate nonahydrate ($Fe(NO_3)_3 \cdot 9H_2O$), ethylene glycol (EG, 99.5%) and potassium carbonate (K_2CO_3, 99.5%, Anhydrous) were purchased from Kishida Chemical Co., Ltd, Osaka, Japan. All chemicals were used as received.

The four metal salts were separately dissolved in water and EG, respectively, to obtain 0.2 M solutions. K_2CO_3 was dissolved in water and EG, respectively, to give 0.6 M aqueous solutions. For synthesizing the multi-element MgAlFeZn hydroxides, both hydrothermal and polyol process were applied. In the hydrothermal process, four metal salts aqueous solutions (2.5 mL each) were mixed with 10 mL K_2CO_3 aqueous solution and sealed in an autoclave. The autoclave was placed in an oven and kept at 100 °C for 2 h. After the hydrothermal treatment, the autoclave was cooled naturally. The product was collected by centrifugation, washed with water and ethanol, and dried in a vacuum oven at 50 °C overnight. The hydrothermal-derived product was denoted as MgAlFeZn-HT. In terms of polyol process, the general synthesis procedure was same, except that all reagents were dissolved in EG and the heat treatment was 150 °C for 2 h. The polyol-derived product was denoted as MgAlFeZn-polyol. Two LDH control samples containing Mg and Al metal species with a Mg/Al molar ratio of 3 were also prepared through hydrothermal and polyol process. The two control samples were named as MgAl-HT and MgAl-polyol, respectively.

Adsorption kinetics study was carried out as follows.[25] 100 mg sample was dropped into 100 mL CR aqueous solution with fixed concentration (*i.e.*, 0.1 and 0.2 mM) under magnetic stirring at room temperature. The suspension was taken at certain time intervals after the mixing and was filtered immediately by a 0.22 μm syringe membrane filter. For adsorption isotherm study, 30 mg sample was suspended in 30 mL CR aqueous solution of adjustable concentration. The suspension was magnetic stirred at room temperature for 24 h. After that, the suspension was filtered using the 0.22 μm syringe membrane filter. The residual concentration of CR in the filtered aqueous solution was calculated by a UV-vis spectrophotometer (JASCO V-76, Tokyo, Japan).

XRD patterns were collected by using an X-ray diffractometer (Bruker D2, Germany) with Cu target (30 kV, 10 mA). The specific surface area of the two samples was measured by using a nitrogen adsorption analyzer (3Flex, Micromeritics, US). The microstructure, composition and elemental distribution of the samples was characterized by using a scanning electron microscope (SEM, SU-70, HITACHI, Japan) and a transmission electron microscope (TEM, JEM 2100F, JEOL, Japan) equipped with an energy-dispersive spectrometer (EDS, Oxford, UK). X-ray photoelectron spectroscopy was obtained from a PHI VersaProbe III.

3. Results and discussions

Fig. 1 shows the normalized XRD patterns of the polyol- and hydrothermal-derived MgAlFeZn hydroxides and MgAl LDH powders. The MgAlFeZn-polyol has three broad diffraction peaks at around 10.7°, 34.8° and 60.5°, indicating its low crystallinity. The relatively sharp increase in baseline at 2θ below 8.5° is due to the systematic error, by carefully analyzing the original XRD patterns of the samples and the blank sample holder (Fig. S1†). The peak position of these three reflections is same with that of the two control samples, *i.e.*, MgAl-polyol and MgAl-HT powders, which both show typical diffraction patterns of LDH with rhombohedral symmetry. These results indicate that the MgAlFeZn-polyol can be indexed as a rhombohedral lattice structure.[42] The three main diffraction peaks of MgAlFeZn-polyol can be assigned to (003), (012), and (110) plane, respectively. The major diffraction peaks of the MgAlFeZn-HT match well with that of MgAl-HT, however, the peak position of each reflection shifts slightly to higher angle. Diffraction peaks of impurities at around 30° and 35.5° are detected. These impurities might be spinel oxides.

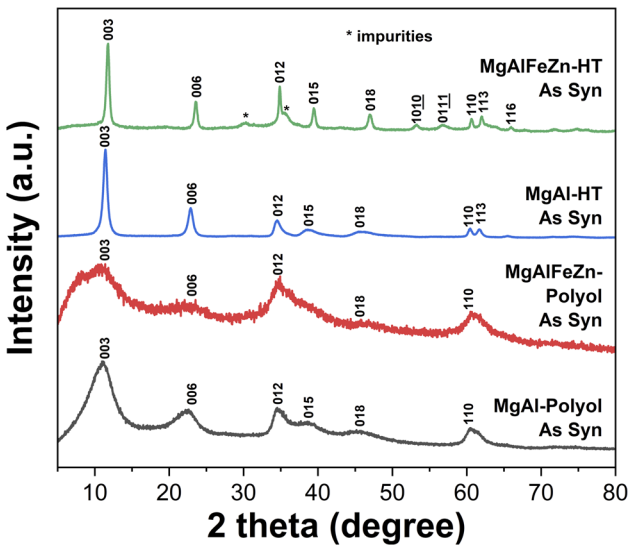

Fig. 1 Normalized XRD patterns of the polyol- and hydrothermal-derived MgAlFeZn hydroxides and MgAl hydroxides.

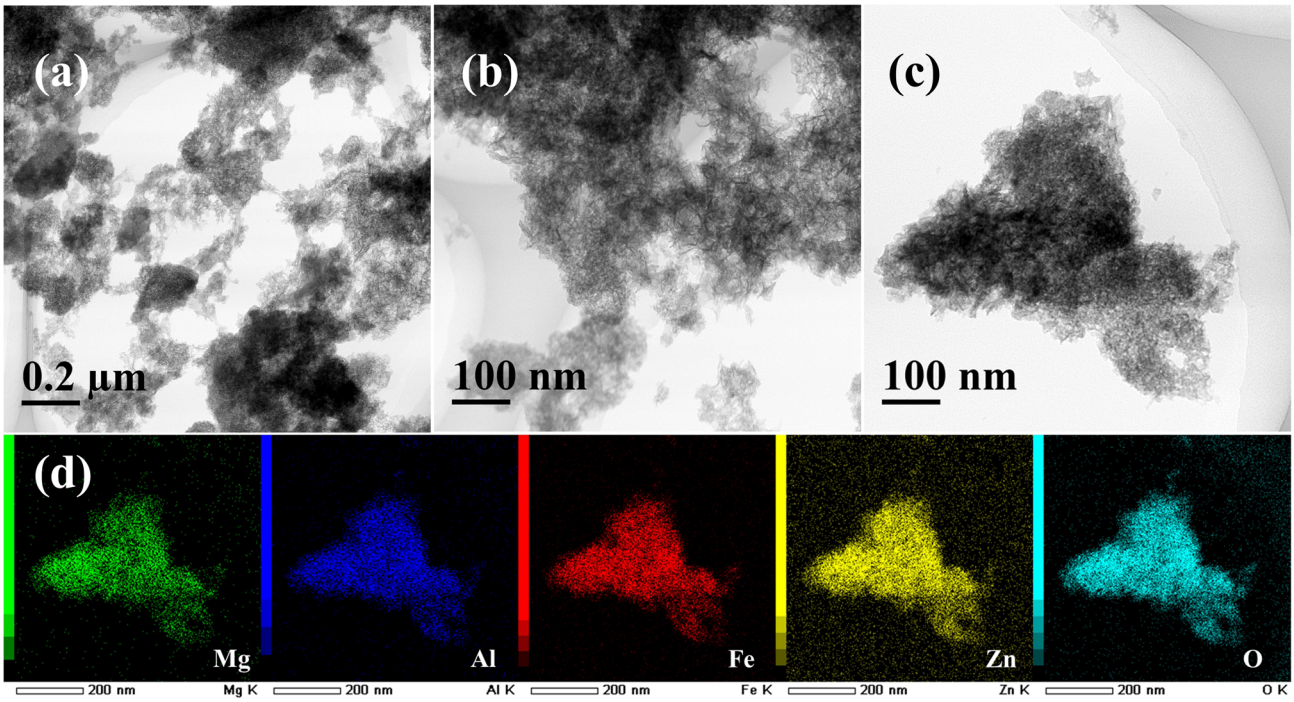

Fig. 2 (a–c) TEM images and (d) EDS mapping of the MgAlFeZn-polyol hydroxides.

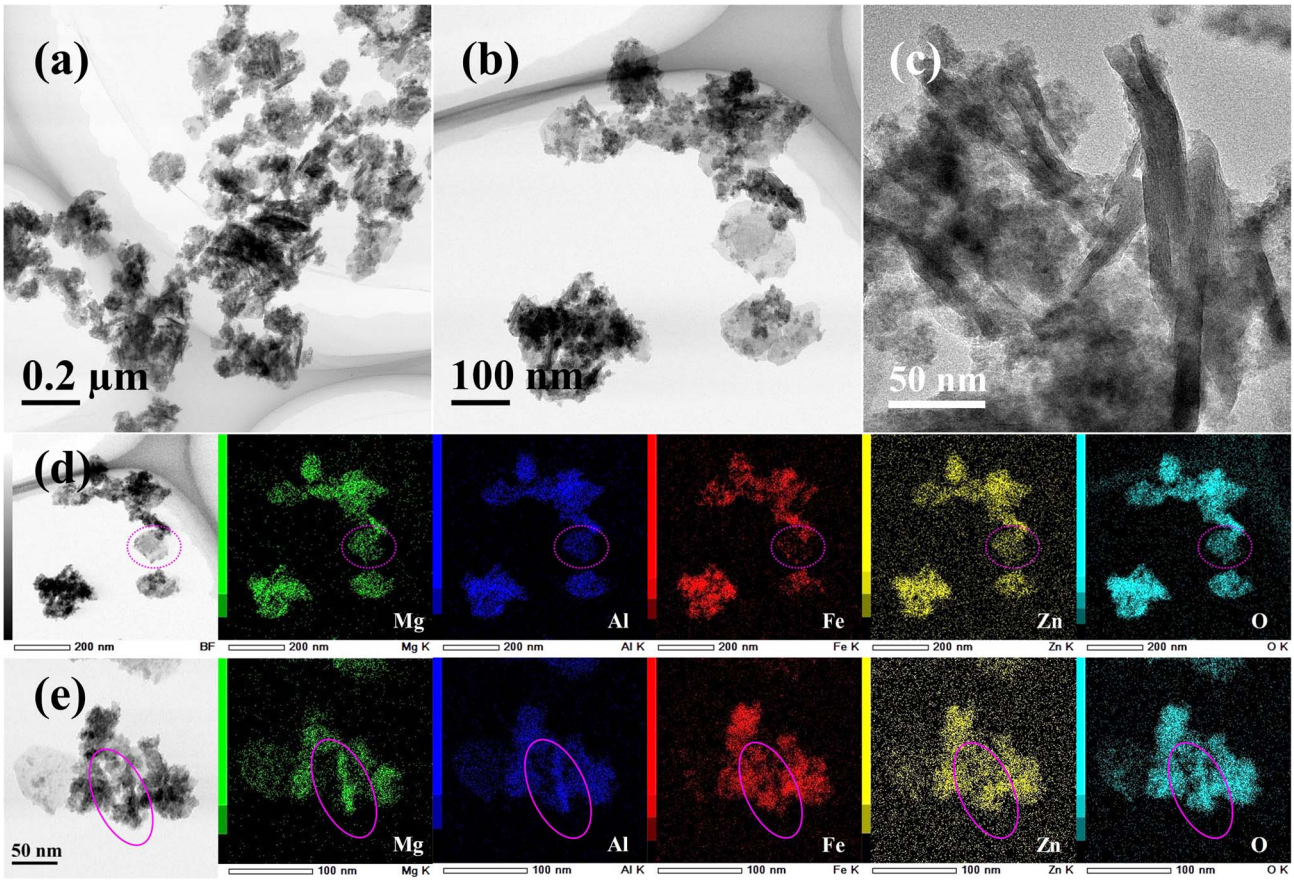

Fig. 3 (a–c) TEM images, (d) and (e) EDS mapping of the MgAlFeZn-HT hydroxides.

Fig. 2 shows the TEM images and elemental maps of the polyol- and hydrothermal-derived MgAlFeZn hydroxides. The MgAlFeZn-polyol is composed of nanosheets of lateral size around 20 nm. Numbers of needle-like morphologies can also be observed in the MgAlFeZn-polyol, as clearly shown in Fig. 2b and c. In Fig. 2d, the corresponding elemental maps of MgAlFeZn-polyol hydroxide show that all the elements are distributed homogeneously. No obvious elemental segregation is observed in MgAlFeZn-polyol, which indicates that these needle-like structures and the nanosheets are compositionally homogeneous. The needle-like shapes in MgAlFeZn-polyol are probably crumpled nanosheets. The composition of the MgAlFeZn-polyol is determined to be Mg 24.2 ± 0.3 at%, Al 25.0 ± 0.6 at%, Fe 19.1 ± 0.6 at%, and Zn 31.7 ± 0.3 at%. The configurational entropy of the MgAlFeZn-polyol is calculated to be 1.4R,[17] where R is the ideal gas constant. This material falls into the category which is so-called medium-entropy material. Multi-element hydroxides MgAlFeZn-polyol demonstrate an extended solubility limit compared with the conventional LDHs.

The MgAlFeZn-HT powder has a similar composition to that of the MgAlFeZn-polyol, *i.e.*, Mg 27.6 ± 0.4 at%, Al 26.5 ± 0.4 at%, Fe 18.1 ± 0.6 at%, and Zn 27.9 ± 0.6 at%. However, three kinds of morphologies exist in the MgAlFeZn-HT. Nanoflakes of lateral size up to 100 nm, elongated nanorods of length up to 200 nm and particulate aggregates can be clearly observed in Fig. 3a–c. The elemental maps in Fig. 3d show that the nanoflakes are deficient in Fe, as marked by dashed circles. As shown in Fig. 3e, the elongated nanorods are rich in Mg, Al and O elements, and deficient in Fe and Zn elements. By combining the XRD result of MgAlFeZn-HT, which has two weak peaks of impurities, the nanorods in MgAlFeZn-HT can probably be considered as Fe and Zn co-doped magnesium aluminate spinel oxides. Based on the XRD and TEM-EDS results, it is confirmed that MgAlFeZn-polyol are homogeneous multi-element hydroxide nanosheets, while MgAlFeZn-HT are mixtures of multi-element hydroxides and spinel oxides. The specific surface area of the MgAlFeZn-polyol and MgAlFeZn-HT is 352.4 and 167.7 $m^2\ g^{-1}$, respectively. The selected four elements Mg, Al, Fe and Zn differ greatly in their K_{sp} values (Table S1†).[41] The results indicate that elemental segregation occurs in hydrothermal process, which can be possibly ascribed to the different cation hydrolysis rates and particle growth rates.[39] The coordinating property and high viscosity of the ethylene glycol provide possibility to mediate the hydrolysis rates and to control the particle growth.[43,44] Such features benefit the homogeneous precipitation of multiple cations through polyol process. It may be possible to obtain homogeneous precipitates of the four cations by optimizing the hydrothermal conditions such as temperature and time. However, it is supposed that the hydrothermal process window is quite narrower than that of polyol process.

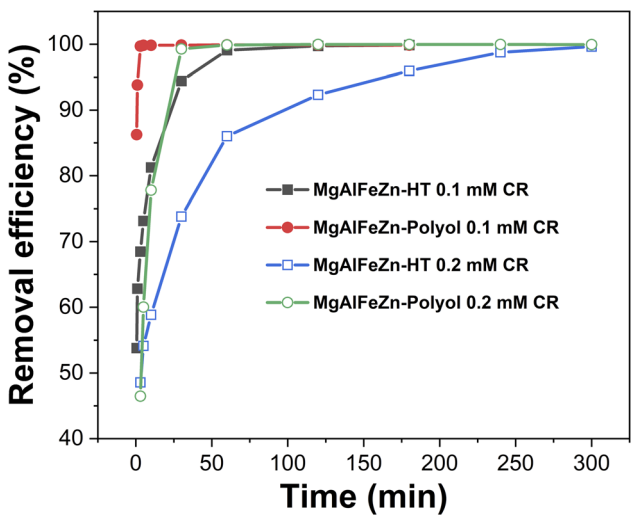

Fig. 4 Time dependency of removal efficiency for polyol- and hydrothermal-derived MgAlFeZn hydroxides in 0.1 mM and 0.2 mM CR aqueous solutions, respectively.

The surface of the polyol- and hydrothermal-derived MgAlFeZn hydroxides is positively charged. The zeta potential value is 11.1 and 15.6 mV for MgAlFeZn-polyol and MgAlFeZn-HT in neutral aqueous suspension, respectively. They were used as adsorbents for CR removal in aqueous solution. Fig. 4 shows the CR removal efficiency for MgAlFeZn hydroxides in 0.1 mM and 0.2 mM CR aqueous solutions. The photographs of the corresponding dye solutions and the UV-vis curves are shown in Fig. S2 and S3.† Regardless of the CR concentrations, both in 0.1 mM and 0.2 mM, the MgAlFeZn-polyol reaches high removal efficiency in less time than MgAlFeZn-HT. In 0.1 mM CR solution, the removal efficiency of MgAlFeZn-polyol is 86.3% in 30 seconds and increases to 99.7% in 3 minutes. The solution then becomes transparent (Fig. S2a and S3a†). For the MgAlFeZn-HT, it requires more than 1 hour to reach the same level in removal efficiency as MgAlFeZn-polyol (Fig. S2b and S3b†). In 0.2 mM CR solution, it takes 30 minutes for the MgAlFeZn-polyol to achieve a removal efficiency over 99% (Fig. S2c and S3c†), and more than 6 hours for the MgAlFeZn-HT (Fig. S2d and S3d†).

Table 1 Adsorption kinetic fitting parameters for the adsorption of CR onto the MgAlFeZn-polyol and MgAlFeZn-HT hydroxides

		Pseudo-second-order model			Pseudo-first-order model		
		k_2 (g mg^{-1} min)	$q_{e,cal}$ (mg g^{-1})	R^2	k_1 (min^{-1})	$q_{e,cal}$ (mg g^{-1})	R^2
MgAlFeZn-HT	0.1 mM CR	1.04×10^{-2}	70.1	0.999	4.03×10^{-2}	18.9	0.957
	0.2 mM CR	8.75×10^{-4}	141.8	0.999	1.58×10^{-2}	67.4	0.992
MgAlFeZn-polyol	0.1 mM CR	6.29×10^{-1}	69.6	0.999	1.00	0.7	0.593
	0.2 mM CR	3.31×10^{-3}	140.6	0.999	2.24×10^{-2}	9.4	0.621

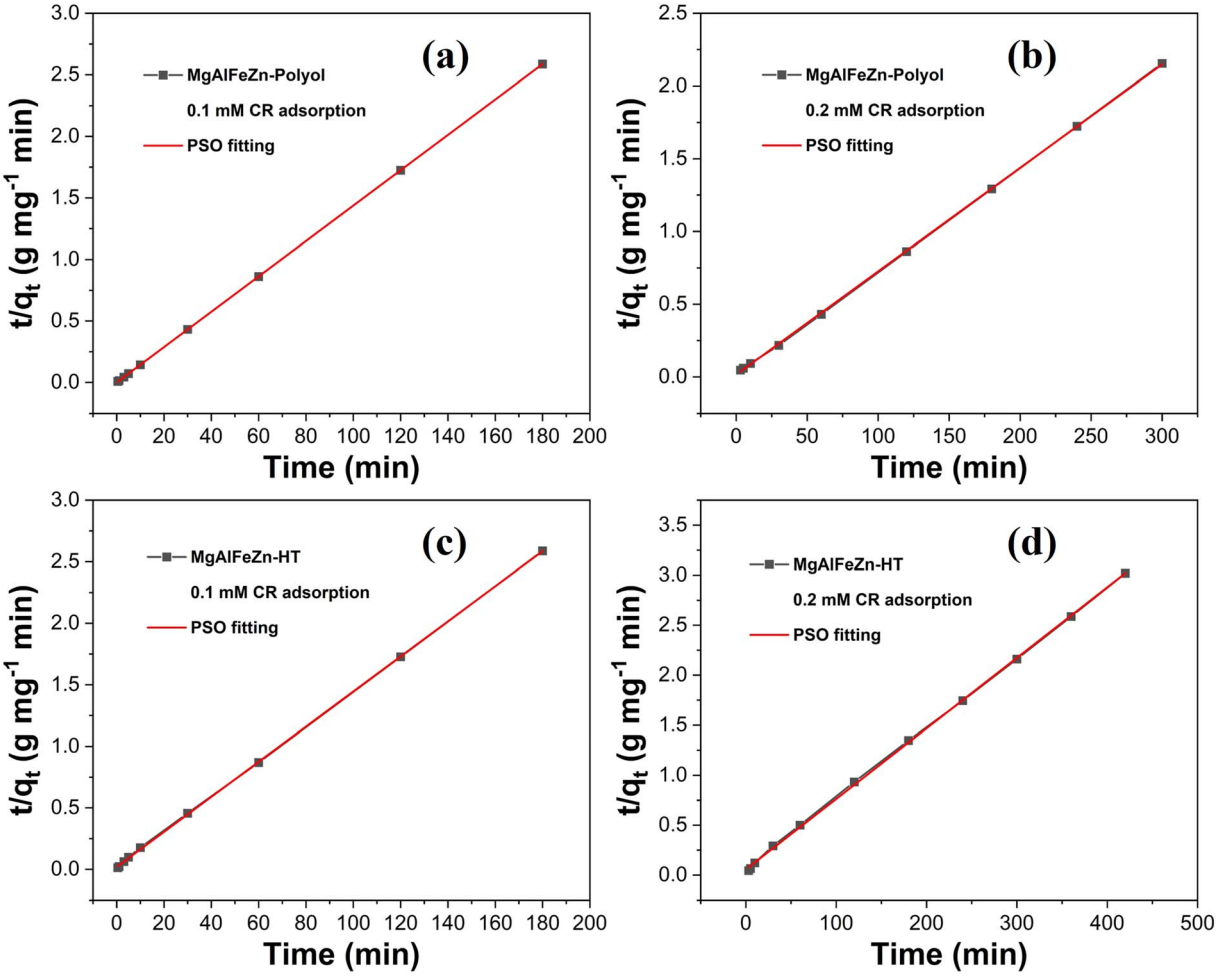

Fig. 5 Pseudo-second-order model fitted curves for CR adsorption onto the MgAlFeZn-polyol (a) 0.1 mM CR, (b) 0.2 mM CR, and MgAlFeZn-HT (c) 0.1 mM CR, (d) 0.2 mM CR.

$$\ln(q_e - q_t) = \ln q_e - k_1 t \quad (1)$$

$$\frac{t}{q_t} = \frac{1}{k_2 q_e^2} + \frac{t}{q_e} \quad (2)$$

The adsorption kinetics were analyzed by using pseudo-first-order (PFO) model (eqn (1)) and pseudo-second-order (PSO) model (eqn (2)).[45] The fitting parameters and curves are shown in Table 1 and Fig. 5, S4.† The high correlation coefficient R^2 and ideal linear fitting curves (Fig. 5) demonstrate that, regardless of the concentration of CR solutions, PSO model is much more appropriate for analyzing the experimental results than PFO model. According to Wang and Guo, one physical meaning of PSO model is that the adsorbent is abundant with active sites.[45] To some extent, the PSO rate constant (k_2) is used to describe the rate of reaching adsorption equilibrium. The MgAlFeZn-polyol has the highest k_2 value of 0.629 g mg^{-1} min in the adsorption of 0.1 mM CR solution. The k_2 ratio for MgAlFeZn-polyol and MgAlFeZn-HT is 60.5, and the ratio decreases to 3.4 in 0.2 mM CR solution. These results indicates that the adsorption of CR is fast at low dye concentration, and it slows down with the increasing dye concentration. In the case of adsorption of high CR concentration solution, numbers of active sites of the adsorbent are occupied by the dye molecules at the first time when mixed in aqueous solution. It takes time

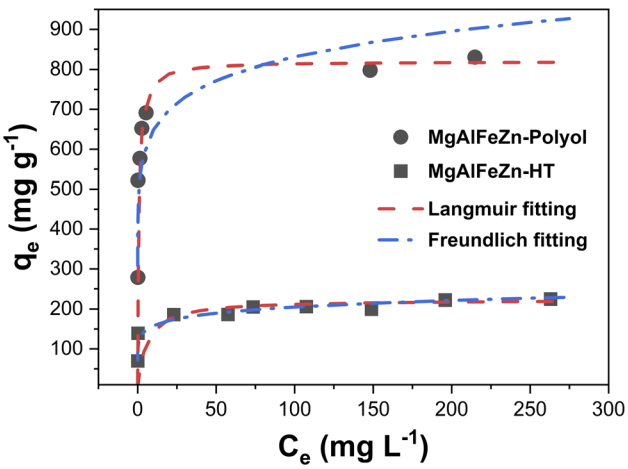

Fig. 6 Adsorption isotherms of CR adsorption onto MgAlFeZn hydroxides and corresponding fitting curves using Langmuir and Freundlich models.

Table 2 Adsorption isotherm fitting parameters for the adsorption of CR onto the MgAlFeZn-polyol and MgAlFeZn-HT hydroxides

	Langmuir model			Freundlich model		
	q_m (mg g^{-1})	K_L (L mg^{-1})	R^2	n	K_F	R^2
MgAlFeZn-HT	223.7	0.18	0.995	8.88	122.0	0.823
MgAlFeZn-polyol	819.7	1.27	0.999	9.29	506.2	0.832

for the dye molecules to diffuse to the vacant active sites, resulting in a decreased adsorption kinetics.[45,46]

Fig. 6 shows the adsorption isotherm curves of the MgAlFeZn-polyol and MgAlFeZn-HT. The MgAlFeZn-polyol shows much higher adsorption capability toward CR than the MgAlFeZn-HT, as clearly shown in Fig. 6. The adsorption isotherm curves are fitted by using Langmuir model (eqn (3)) and Freundlich model (eqn (4)), respectively.[47] The adsorption isotherm fitting parameters are listed in Table 2. The high R^2 values obtained from Langmuir model fitting indicates that Langmuir model rather than Freundlich model is reasonable to illustrate the interactions between the dye molecules and the adsorbents. The Langmuir model implies that the dye adsorption occurs on the homogeneous surface of the adsorbents.[47] The calculated maximum adsorption capacity (q_m) is 819.7 mg g^{-1} for the MgAlFeZn-polyol, much higher than that for the MgAlFeZn-HT (223.7 mg g^{-1}).

$$\frac{C_e}{q_e} = \frac{C_e}{q_m} + \frac{1}{q_m K_L} \quad (3)$$

$$\ln q_e = \ln K_F + \frac{\ln C_e}{n} \quad (4)$$

XPS was used to characterize the surface chemical states of the polyol- and hydrothermal-derived hydroxides, as shown in Fig. 7 and S5.† The survey spectra in Fig. S5a† confirm the presence of the targeted metal species. Among the four metal elements, except for Fe, the valence states of the Mg, Al, and Zn elements are unlikely to change, as shown in Fig. S5b and c.† For the Fe 2p spectra of the MgAlFeZn-polyol (Fig. 7a) and MgAlFeZn-HT (Fig. 7c), the $2p_{3/2}$ peak can be fitted into Fe^{2+} $2p_{3/2}$ at 710.2 eV and Fe^{3+} $2p_{3/2}$ at 711.9 eV.[25,26] The proportion of Fe^{2+} in Fe 2p spectrum of MgAlFeZn-polyol is a little bit higher

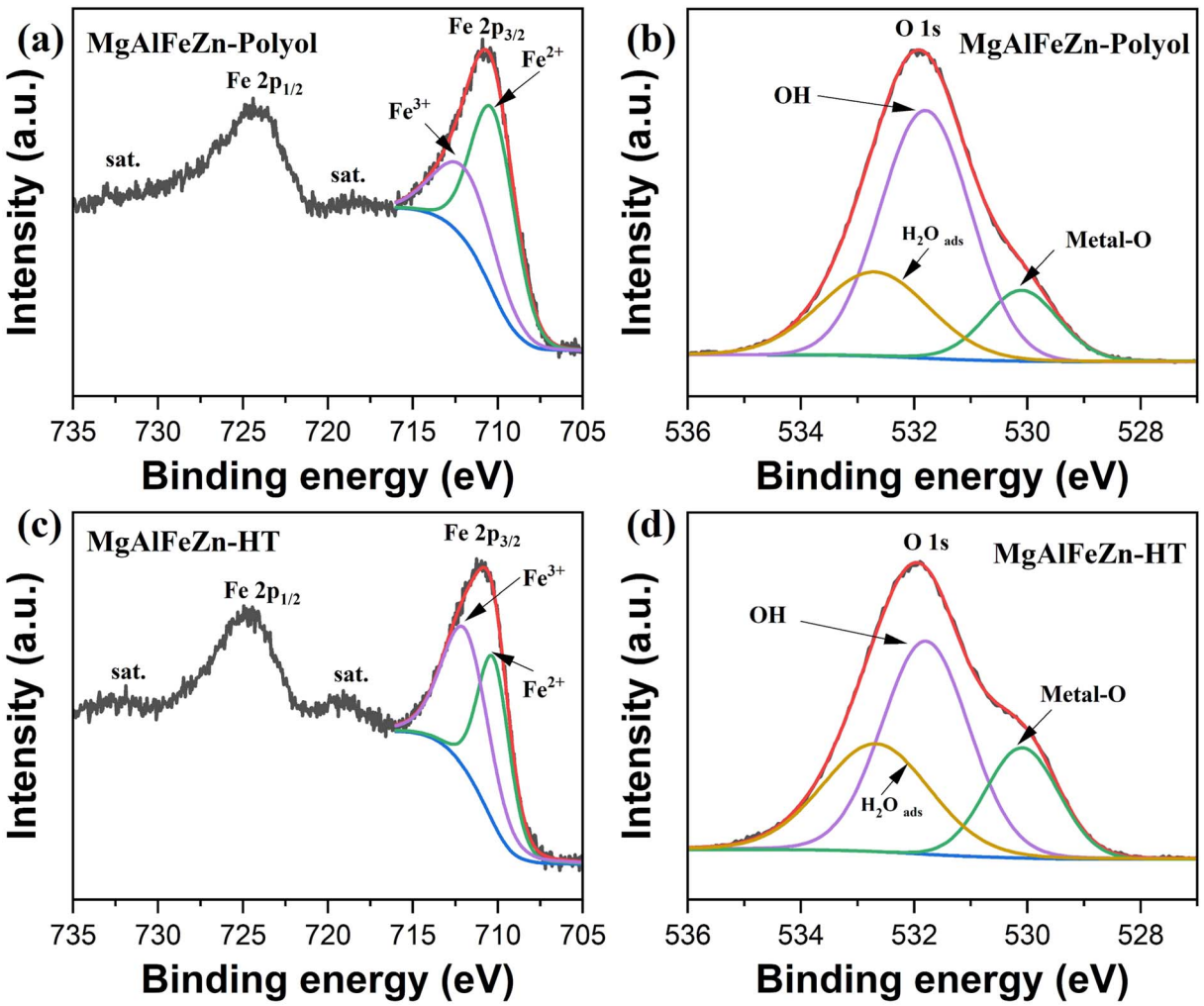

Fig. 7 (a) Fe 2p and (b) O 1s XPS spectra of the MgAlFeZn-polyol. (c) Fe 2p and (d) O 1s XPS spectra of the MgAlFeZn-HT.

than that of MgAlFeZn-HT. This slight difference might be due partially to the reducing feature of the polyol.[43] Such difference is also consistent with their difference in zeta potential, that MgAlFeZn-polyol has a lower zeta potential than MgAlFeZn-HT. In terms of the O 1s spectra of MgAlFeZn-polyol (Fig. 7b) and MgAlFeZn-HT (Fig. 7d), three fitted peaks at 530.1, 531.8, and 532.8 eV can be assigned to lattice metal–O bonding, OH^- and adsorbed H_2O, respectively.[25,48] The proportion of metal–O bonding in MgAlFeZn-HT is slightly higher, while the proportion of OH^- is slightly lower than that in MgAlFeZn-polyol. Such difference agrees well with the fact that the MgAlFeZn-HT contains spinel oxides as secondary phase. On the basis of the XPS analyses, there is not obvious difference in the surface chemical states between MgAlFeZn-polyol and MgAlFeZn-HT. Charge transfer-based mechanism is possibly vague in interpreting the adsorption behavior of MgAlFeZn hydroxides. The high specific surface area of the MgAlFeZn-polyol (352.4 $m^2\ g^{-1}$) should be one of the main factors responsible for its excellent CR adsorption capability.

By analyzing the structural change for the MgAlFeZn hydroxides before and after CR adsorption, it can provide details to under the adsorption mechanism. The XRD patterns of the polyol- and hydrothermal-derived MgAlFeZn hydroxides after adsorbing CR are shown in Fig. 8. For better comparison, the XRD patterns of the as synthesized MgAlFeZn hydroxides, which are already presented in Fig. 1, are once again provided in Fig. 8. As aforementioned in Fig. 1, both the XRD patterns of MgAlFeZn-polyol and MgAlFeZn-HT can be indexed to rhombohedral lattice structure. Adsorbing CR does not change their crystal structure. The peak position of each reflection are exactly the same as the one prior to CR adsorption. In terms of MgAlFeZn-polyol, it is stable in aqueous conditions as no obvious changes in the XRD patterns after dispersion in pure water (Fig. S6†). Its basal reflections of (003) and (006) planes are obvious, and the non-basal reflections at intermediate angles are identifiable after CR adsorption. According to the (003) peak width of MgAlFeZn-polyol and Scherrer equation,[49] the crystallite size perpendicular to the basal plane (*i.e.*, the thickness of the nanosheets) increases after adsorption. The XRD results imply that stacking of the thin nanosheets occurs during the procedure. In terms of the MgAlFeZn-HT, there is no obvious change in their XRD patterns before and after CR adsorption, indicating that the structure of MgAlFeZn-HT is stable, and the CR adsorption occurs on the surface rather than through intercalation.

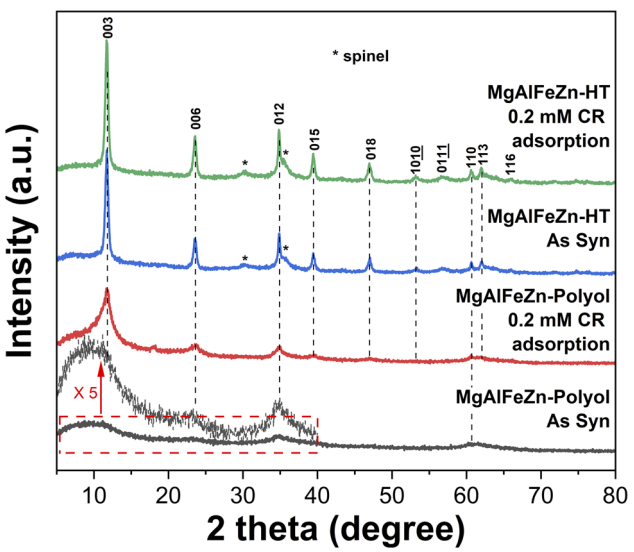

Fig. 8 XRD patterns of the MgAlFeZn hydroxides and the corresponding dried powders after reaching adsorption equilibrium in 0.2 mM CR aqueous solution.

4. Conclusions

In summary, the multi-element hydroxides composed of Mg, Al, Fe and Zn elements are synthesized through polyol and hydrothermal processes. Polyol process is proved to be a powerful method to mix multiple elements differing greatly in solubility products without phase separation at nanoscale. The hydrothermal-derived MgAlFeZn hydroxides are mixtures of plate-like hydroxide layers and rod-like spinel oxides. The polyol-derived MgAlFeZn hydroxides are nanosheets of homogeneous elemental distribution and high specific surface area (352.4 $m^2\ g^{-1}$). The high specific surface area of these hydroxides guarantees them as excellent adsorbents for adsorbing Congo red in aqueous solution. The MgAlFeZn hydroxides nanosheets show faster adsorption kinetics and higher maximum adsorption capability (819.7 mg g^{-1}) toward Congo red than the hydrothermal-derived MgAlFeZn hydroxides (223.7 mg g^{-1}).

Conflicts of interest

There are no conflicts to declare.

Acknowledgements

This research work was financially supported by OU Master Plan Implementation Project promoted under Osaka University, a Grant-in-Aid for the Cooperative Research Project of Design & Engineering by Joint Inverse Innovation for Materials Architecture (DEJI^{2}MA) of the Ministry of Education, Culture, Sports, Science and Technology (MEXT), and JSPS KAKENHI Grant Number 21H01637, Japan. Dr Sadahiro Yagishita and Dr Keisuke Fujita from Daiichi Kigenso Kagaku Kogyo Co., Ltd is acknowledged for taking Zeta potential measurements.

References

1 X. Duan and D. G. Evans, *Layered Double Hydroxides*, Springer Berlin, Heidelberg, 2006.
2 T. Sudare, K. Kawaguchi, K. Yamaguchi, K. Hirono, M. Tipplook, H. Tanaka, F. Hayashi and K. Teshima, *Chem. Mater.*, 2022, **34**, 10681–10690.
3 D. Zhou, P. Li, X. Lin, A. McKinley, Y. Kuang, W. Liu, W.-F. Lin, X. Sun and X. Duan, *Chem. Soc. Rev.*, 2021, **50**, 8790–8817.

4 Z.-H. Xie, H.-Y. Zhou, C.-S. He, Z.-C. Pan, G. Yao and B. Lai, *Chem. Eng. J.*, 2021, **414**, 128713.
5 X. Jia, S. Gao, T. Liu, D. Li, P. Tang and Y. Feng, *Electrochim. Acta*, 2017, **245**, 59–68.
6 T. Hu, Z. Gu, G. R. Williams, M. Strimaite, J. Zha, Z. Zhou, X. Zhang, C. Tan and R. Liang, *Chem. Soc. Rev.*, 2022, **51**, 6126–6176.
7 C. M. Rost, E. Sachet, T. Borman, A. Moballegh, E. C. Dickey, D. Hou, J. L. Jones, S. Curtarolo and J.-P. Maria, *Nat. Commun.*, 2015, **6**, 8485.
8 C. Oses, C. Toher and S. Curtarolo, *Nat. Rev. Mater.*, 2020, **5**, 295–309.
9 E. P. George, D. Raabe and R. O. Ritchie, *Nat. Rev. Mater.*, 2019, **4**, 515–534.
10 W.-Y. Huo, S.-Q. Wang, W.-H. Zhu, Z.-L. Zhang, F. Fang, Z.-H. Xie and J.-Q. Jiang, *Tungsten*, 2021, **3**, 161–180.
11 Z. Wang, Z.-T. Li, S.-J. Zhao and Z.-G. Wu, *Tungsten*, 2021, **3**, 131–142.
12 L. Zhou, J.-X. Liu, T.-Z. Tu, Y. Wu and G.-J. Zhang, *J. Adv. Ceram.*, 2023, **12**, 111–121.
13 X.-T. Xin, W. Bao, X.-G. Wang, X.-J. Guo, Y. Lu, C. Zhu, J.-X. Liu, Q. Li, F. Xu and G.-J. Zhang, *J. Adv. Ceram.*, 2023, **12**, 916–929.
14 T.-Z. Tu, J.-X. Liu, Y. Wu, L. Zhou, Y. Liang and G.-J. Zhang, *J. Adv. Ceram.*, 2023, **12**, 861–872.
15 Y. Qin, J.-X. Liu, Y. Liang and G.-J. Zhang, *J. Adv. Ceram.*, 2022, **11**, 1082–1092.
16 Y.-G. Yan, D. Lu and K. Wang, *Tungsten*, 2023, **5**, 32–49.
17 Q. Zhang, Y. Hu, H. Wu, X. Zhao, M. Wang, S. Wang, R. Feng, Q. Chen, F. Song, M. Chen and P. Liu, *ACS Nano*, 2023, **17**, 1485–1494.
18 Y. G. Yan and K. Wang, *Tungsten*, 2023, **5**, 531–538.
19 X. Yu, B. Wang, C. Wang, C. Zhuang, Y. Yao, Z. Li, C. Wu, J. Feng and Z. Zou, *Small*, 2021, **17**, 2103412.
20 L. Zhang, W. Cai and N. Bao, *Adv. Mater.*, 2021, **33**, 2100745.
21 L. He, N. Wang, B. Sun, L. Zhong, M. Yao, W. Hu and S. Komarneni, *J. Cleaner Prod.*, 2022, **356**, 131680.
22 A. J. Knorpp, A. Zawisza, S. Huangfu, A. Borzì, A. H. Clark, D. Kata, T. Graule and M. Stuer, *RSC Adv.*, 2022, **12**, 26362–26371.
23 T. Xue, Y. Wang, L. Yang, Z. Li, Y. Gao and Q. Wang, *Catalysts*, 2023, **13**, 119.
24 F. Li, S.-K. Sun, Y. Chen, T. Naka, T. Hashishin, J. Maruyama and H. Abe, *Nanoscale Adv.*, 2022, **4**, 2468–2478.
25 F. Li, N. Kannari, J. Maruyama, K. Sato and H. Abe, *J. Hazard. Mater.*, 2023, **447**, 130803.
26 M. Han, C. Wang, J. Zhong, J. Han, N. Wang, A. Seifitokaldani, Y. Yu, Y. Liu, X. Sun, A. Vomiero and H. Liang, *Appl. Catal., B*, 2022, **301**, 120764.
27 C. L. Dupont, G. Grass and C. Rensing, *Metallomics*, 2011, **3**, 1109–1118.
28 S. L. Holland and S. V. Avery, *Metallomics*, 2011, **3**, 1119–1123.
29 F. Barras and M. Fontecave, *Metallomics*, 2011, **3**, 1130–1134.
30 L. Macomber and R. P. Hausinger, *Metallomics*, 2011, **3**, 1153–1162.
31 G. Grass, L. Rensing and C. Rensing, *Metallomics*, 2011, **3**, 1095–1097.
32 Y.-W. Huang, C.-h. Wu and R. S. Aronstam, *Materials*, 2010, **3**, 4842–4859.
33 F. Lu and D. Astruc, *Coord. Chem. Rev.*, 2018, **356**, 147–164.
34 S. K. Nemani, M. Torkamanzadeh, B. C. Wyatt, V. Presser and B. Anasori, *Commun. Mater.*, 2023, **4**, 16.
35 M. Hao, J. Chen, J. Chen, K. Wang, J. Wang, F. Lei, P. Hao, X. Sun, J. Xie and B. Tang, *J. Colloid Interface Sci.*, 2023, **642**, 41–52.
36 T. G. Ritter, A. H. Phakatkar, M. G. Rasul, M. T. Saray, L. V. Sorokina, T. Shokuhfar, J. M. Gonçalves and R. Shahbazian-Yassar, *Cell Rep. Phys. Sci.*, 2022, **3**, 100847.
37 K. Gu, X. Zhu, D. Wang, N. Zhang, G. Huang, W. Li, P. Long, J. Tian, Y. Zou, Y. Wang, R. Chen and S. Wang, *J. Energy Chem.*, 2021, **60**, 121–126.
38 A. Miura, S. Ishiyama, D. Kubo, N. C. Rosero-Navarro and K. Tadanaga, *J. Ceram. Soc. Jpn.*, 2020, **128**, 336–339.
39 Y. Wu, D. Wang and Y. Li, *Sci. China Mater.*, 2016, **59**, 938–996.
40 G. R. Dey, C. R. McCormick, S. S. Soliman, A. J. Darling and R. E. Schaak, *ACS Nano*, 2023, **17**, 5943–5955.
41 J. G. Speight, *Lange's Handbook of Chemistry*, McGraw-Hill Education, New York, 17th edn, 2017.
42 D. G. Evans and R. C. T. Slade, in *Layered Double Hydroxides*, ed. X. Duan and D. G. Evans, Springer Berlin Heidelberg, Berlin, Heidelberg, 2006, pp. 1–87, DOI: **10.1007/430_005**.
43 F. Fiévet, S. Ammar-Merah, R. Brayner, F. Chau, M. Giraud, F. Mammeri, J. Peron, J. Y. Piquemal, L. Sicard and G. Viau, *Chem. Soc. Rev.*, 2018, **47**, 5187–5233.
44 H. Dong, Y. C. Chen and C. Feldmann, *Green Chem.*, 2015, **17**, 4107–4132.
45 J. Wang and X. Guo, *J. Hazard. Mater.*, 2020, **390**, 122156.
46 H. Hou, R. Zhou, P. Wu and L. Wu, *Chem. Eng. J.*, 2012, **211–212**, 336–342.
47 M. A. Al-Ghouti and D. A. Da'ana, *J. Hazard. Mater.*, 2020, **393**, 122383.
48 C. Zhong, J. Zhang, L. Zhang, Y. Tu, H. Song, L. Du and Z. Cui, *ACS Energy Lett.*, 2023, **8**, 1455–1462.
49 U. Holzwarth and N. Gibson, *Nat. Nanotechnol.*, 2011, **6**, 534.